Published for SISSA by Springer

Received: June 6, 2023
Accepted: September 8, 2023
Published: September 21, 2023

Measurement of CP asymmetries and branching-fraction ratios for $B^{\pm} \to DK^{\pm}$ and $D\pi^{\pm}$ with $D \to K^0_S K^{\pm}\pi^{\mp}$ using Belle and Belle II data

The Belle and Belle II collaborations
https://belle.kek.jp/

I. Adachi, L. Aggarwal, H. Aihara, N. Akopov, A. Aloisio, N. Anh Ky, D. M. Asner, T. Aushev, V. Aushev, M. Aversano, R. Ayad, V. Babu, H. Bae, S. Bahinipati, P. Bambade, Sw. Banerjee, M. Barrett, J. Baudot, M. Bauer, A. Baur, A. Beaubien, J. Becker, P. K. Behera, J. V. Bennett, F. U. Bernlochner, V. Bertacchi, M. Bertemes, E. Bertholet, M. Bessner, S. Bettarini, B. Bhuyan, F. Bianchi, T. Bilka, D. Biswas, A. Bobrov, D. Bodrov, A. Bolz, A. Bondar, J. Borah, A. Bozek, M. Bračko, P. Branchini, R. A. Briere, T. E. Browder, A. Budano, S. Bussino, M. Campajola, L. Cao, G. Casarosa, C. Cecchi, J. Cerasoli, M.-C. Chang, P. Chang, R. Cheaib, P. Cheema, V. Chekelian, B. G. Cheon, K. Chilikin, K. Chirapatpimol, H.-E. Cho, K. Cho, S.-K. Choi, Y. Choi, S. Choudhury, J. Cochran, L. Corona, L. M. Cremaldi, S. Das, F. Dattola, E. De La Cruz-Burelo, S. A. De La Motte, G. De Nardo, M. De Nuccio, G. De Pietro, R. de Sangro, M. Destefanis, S. Dey, A. De Yta-Hernandez, R. Dhamija, A. Di Canto, F. Di Capua, J. Dingfelder, Z. Doležal, I. Domínguez Jiménez, T. V. Dong, M. Dorigo, K. Dort, S. Dreyer, S. Dubey, G. Dujany, P. Ecker, D. Epifanov, P. Feichtinger, T. Ferber, D. Ferlewicz, T. Fillinger, C. Finck, G. Finocchiaro, A. Fodor, F. Forti, A. Frey, B. G. Fulsom, A. Gabrielli, E. Ganiev, M. Garcia-Hernandez, R. Garg, A. Garmash, G. Gaudino, V. Gaur, A. Gaz, A. Gellrich, G. Ghevondyan, D. Ghosh, H. Ghumaryan, G. Giakoustidis, R. Giordano, A. Giri, B. Gobbo, R. Godang, O. Gogota, P. Goldenzweig, W. Gradl,

https://doi.org/10.1007/JHEP09(2023)146

JHEP09(2023)146

E. Graziani, D. Greenwald, Z. Gruberová, T. Gu, Y. Guan, K. Gudkova, S. Halder, Y. Han, T. Hara, K. Hayasaka, S. Hazra, M. T. Hedges, I. Heredia de la Cruz, M. Hernández Villanueva, A. Hershenhorn, T. Higuchi, E. C. Hill, M. Hoek, M. Hohmann, W.-S. Hou, C.-L. Hsu, T. Iijima, K. Inami, N. Ipsita, A. Ishikawa, S. Ito, R. Itoh, M. Iwasaki, P. Jackson, W. W. Jacobs, D. E. Jaffe, E.-J. Jang, Q. P. Ji, S. Jia, Y. Jin, A. Johnson, H. Junkerkalefeld, A. B. Kaliyar, J. Kandra, K. H. Kang, G. Karyan, T. Kawasaki, F. Keil, C. Ketter, C. Kiesling, C.-H. Kim, D. Y. Kim, K.-H. Kim, Y.-K. Kim, H. Kindo, K. Kinoshita, P. Kodyš, T. Koga, S. Kohani, K. Kojima, A. Korobov, S. Korpar, E. Kovalenko, R. Kowalewski, T. M. G. Kraetzschmar, P. Križan, P. Krokovny, T. Kuhr, M. Kumar, K. Kumara, T. Kunigo, A. Kuzmin, Y.-J. Kwon, S. Lacaprara, Y.-T. Lai, T. Lam, L. Lanceri, J. S. Lange, M. Laurenza, K. Lautenbach, R. Leboucher, F. R. Le Diberder, P. Leitl, D. Levit, P. M. Lewis, C. Li, L. K. Li, J. Libby, Q. Y. Liu, Z. Q. Liu, D. Liventsev, S. Longo, T. Lueck, T. Luo, C. Lyu, Y. Ma, M. Maggiora, S. P. Maharana, R. Maiti, S. Maity, G. Mancinelli, R. Manfredi, E. Manoni, M. Mantovano, D. Marcantonio, C. Marinas, C. Martellini, A. Martini, T. Martinov, L. Massaccesi, M. Masuda, T. Matsuda, K. Matsuoka, D. Matvienko, S. K. Maurya, J. A. McKenna, R. Mehta, F. Meier, M. Merola, F. Metzner, M. Milesi, C. Miller, M. Mirra, K. Miyabayashi, R. Mizuk, G. B. Mohanty, N. Molina-Gonzalez, S. Mondal, S. Moneta, H.-G. Moser, M. Mrvar, R. Mussa, I. Nakamura, Y. Nakazawa, A. Narimani Charan, M. Naruki, Z. Natkaniec, A. Natochii, L. Nayak, G. Nazaryan, N. K. Nisar, S. Nishida, S. Ogawa, H. Ono, Y. Onuki, P. Oskin, F. Otani, P. Pakhlov, G. Pakhlova, A. Paladino, A. Panta, E. Paoloni, S. Pardi, K. Parham, H. Park, S.-H. Park, A. Passeri, S. Patra, S. Paul, T. K. Pedlar, I. Peruzzi, R. Peschke, R. Pestotnik, F. Pham, M. Piccolo, L. E. Piilonen, P. L. M. Podesta-Lerma, T. Podobnik, S. Pokharel, C. Praz, S. Prell, E. Prencipe, M. T. Prim, H. Purwar, N. Rad, P. Rados, G. Raeuber, S. Raiz, M. Reif, S. Reiter, M. Remnev, I. Ripp-Baudot, G. Rizzo, S. H. Robertson, M. Roehrken, J. M. Roney, A. Rostomyan, N. Rout, G. Russo, D. Sahoo, S. Sandilya, A. Sangal, L. Santelj, Y. Sato, V. Savinov, B. Scavino, C. Schmitt, G. Schnell, M. Schnepf, C. Schwanda, A. J. Schwartz, Y. Seino, A. Selce, K. Senyo, J. Serrano, M. E. Sevior, C. Sfienti, W. Shan, C. Sharma, X. D. Shi, T. Shillington, J.-G. Shiu, D. Shtol, A. Sibidanov, F. Simon, J. B. Singh, J. Skorupa, R. J. Sobie, M. Sobotzik, A. Soffer, A. Sokolov, E. Solovieva, S. Spataro, B. Spruck, M. Starič, P. Stavroulakis, S. Stefkova, Z. S. Stottler, R. Stroili, M. Sumihama, K. Sumisawa, W. Sutcliffe, H. Svidras, M. Takahashi, M. Takizawa, U. Tamponi, K. Tanida, F. Tenchini, A. Thaller, O. Tittel, R. Tiwary,

JHEP09(2023)146

D. Tonelli, E. Torassa, K. Trabelsi, I. Tsaklidis, M. Uchida, I. Ueda, T. Uglov, K. Unger, Y. Unno, K. Uno, S. Uno, P. Urquijo, Y. Ushiroda, S. E. Vahsen, R. van Tonder, G. S. Varner, K. E. Varvell, M. Veronesi, V. S. Vismaya, L. Vitale, V. Vobbilisetti, R. Volpe, B. Wach, M. Wakai, S. Wallner, E. Wang, M.-Z. Wang, Z. Wang, A. Warburton, M. Watanabe, S. Watanuki, M. Welsch, C. Wessel, E. Won, X. P. Xu, B. D. Yabsley, S. Yamada, W. Yan, S. B. Yang, J. H. Yin, K. Yoshihara, C. Z. Yuan, Y. Yusa, L. Zani, Y. Zhang, V. Zhilich, J. S. Zhou, Q. D. Zhou, V. I. Zhukova and R. Žlebčík

E-mail: xiaodong.shi@kek.jp, coll-publications@belle2.org

Abstract: We measure CP asymmetries and branching-fraction ratios for $B^{\pm} \to DK^{\pm}$ and $D\pi^{\pm}$ decays with $D \to K^0_S K^{\pm}\pi^{\mp}$, where D is a superposition of D^0 and $\bar{D}^0$. We use the full data set of the Belle experiment, containing 772×10^6 $B\bar{B}$ pairs, and data from the Belle II experiment, containing 387×10^6 $B\bar{B}$ pairs, both collected in electron-positron collisions at the $\Upsilon(4S)$ resonance. Our results provide model-independent information on the unitarity triangle angle ϕ_3.

Keywords: B Physics, CKM Angle Gamma, CP Violation, e^+-e^- Experiments

ArXiv ePrint: 2306.02940

JHEP09(2023)146

Contents

JHEP09(2023)146

1 Introduction

In the Standard Model, *CP* violation is described by a single irreducible complex phase of the Cabibbo-Kobayashi-Maskawa (CKM) quark-mixing matrix [1, 2]. The CKM matrix is unitary, so $V_{ud}V_{ub}^* + V_{cd}V_{cb}^* + V_{td}V_{tb}^* = 0$, where V_{ij} is the CKM matrix element coupling quark flavour i to quark flavour j. This condition, represented by a triangle in the complex plane, provides a promising way to verify the Standard Model by testing the closure of the triangle. The interior angle ϕ_3 (also known as γ), defined as $\arg(-V_{ud}V_{ub}^*/V_{cd}V_{cb}^*)$, is independent of top-quark couplings and a benchmark of the Standard Model. Through the interference of $b \to c\bar{u}s$ and $b \to u\bar{c}s$ transition amplitudes in tree-level b-hadron decays, where non-Standard-Model effects are negligible [3], ϕ_3 can be studied in a theoretically reliable way [4]. An improved direct measurement of ϕ_3 would provide a key input for Standard Model predictions, which can be compared with predictions of other measured observables that are sensitive to new particles and interactions.

The world average of ϕ_3 measurements, $(65.9^{+3.3}_{-3.5})^\circ$ [5], in which the LHCb experiment contributes most, is dominated by studies of the interference of $B^\pm \to D^0K^\pm$ and $B^\pm \to \overline{D}^0K^\pm$ decays in which the D^0 and $\overline{D}^0$ decay to a common final state [6–8]. Grossman, Ligeti, and Soffer (GLS) proposed a method to measure ϕ_3 with singly Cabibbo-suppressed decays of D mesons, $D \to K^0_S K^\pm\pi^\mp$ [9], where D is a superposition of D^0 and $\overline{D}^0$ mesons.

Experimentally, one measures seven observables to access ϕ_3, including four CP asymmetries and three branching-fraction ratios in $B^\pm \to Dh^\pm$ decays, where h is a pion or kaon. From these, the ϕ_3-related information is extracted without model dependent uncertainties from the amplitude model of D decay. However, information about the $D \to K^0_S K^\pm \pi^\mp$ dynamics is necessary. The CLEO experiment measured this information using all such D decays and also using only decays in which the $K^0_S \pi^\mp$ pair has a mass within $100\,\mathrm{MeV}/c^2$ of the known $K^*(892)^\mp$ mass [10].[1] In that region, the interference of $B^\pm \to D^0 h^\pm$ and $B^\pm \to \overline{D}^0 h^\pm$ decays is expected to be enhanced due to the large coherence factor in $D \to K^0_S K^\pm \pi^\mp$ decays, possibly leading to a more precise determination of ϕ_3. The principal experimental challenge is extracting the signal given the small branching fractions of these channels.

The LHCb collaboration reported the most precise GLS measurement to date [11]. In this paper, we present a similar measurement for $B^\pm \to DK^\pm$ and $B^\pm \to D\pi^\pm$ using 772×10^6 $B\overline{B}$ pairs collected by the Belle experiment [12] and 387×10^6 $B\overline{B}$ pairs collected by the Belle II experiment [13], produced in electron-positron collisions at the $\Upsilon(4S)$ resonance.[2] We fit to the distributions of two signal-discriminating observables, simultaneously in both data sets and all channels to extract the seven GLS observables. An additional measurement restricted to a $K^{*\pm}$-enriched region of the D meson phase space is also reported, as well as results based on the Belle data only.

2 Formalism

We categorise $B^\pm \to Dh^\pm$ followed by $D \to K^0_S K^\pm \pi^\mp$ as same-sign (SS) or opposite-sign (OS) decays according to the charge of the $K^\pm$ produced by the D meson relative to the charge of the $B^\pm$ meson. The four CP asymmetries are

$$\mathcal{A}_m^{Dh} \equiv \frac{N_m^{Dh^-} - N_m^{Dh^+}}{N_m^{Dh^-} + N_m^{Dh^+}} \qquad \text{with} \qquad h = \pi, K, \tag{2.1}$$

where $N_m^{Dh^\pm}$ is the number of $B^\pm \to Dh^\pm$ decays, and m denotes the decay type, which is either SS or OS. The three branching-fraction ratios are

$$\mathcal{R}_m^{DK/D\pi} \equiv \frac{N_m^{DK^-} + N_m^{DK^+}}{N_m^{D\pi^-} + N_m^{D\pi^+}} \tag{2.2}$$

and

$$\mathcal{R}_{\mathrm{SS/OS}}^{D\pi} \equiv \frac{N_{\mathrm{SS}}^{D\pi^-} + N_{\mathrm{SS}}^{D\pi^+}}{N_{\mathrm{OS}}^{D\pi^-} + N_{\mathrm{OS}}^{D\pi^+}}. \tag{2.3}$$

[1] The $K^*(892)^\pm$ is henceforth referred to as $K^{*\pm}$.

[2] Here, B indicates either a B^+ or B^0.

JHEP09(2023)146

The relations between the seven observables and ϕ_3 are given by the following equations:

$$
\begin{aligned}
\mathcal{A}_{\rm SS}^{DK} &= \frac{2r_B^{DK} r_D \kappa_D \sin(\delta_B^{DK} - \delta_D)\sin\phi_3}{1 + (r_B^{DK})^2 r_D^2 + 2r_B^{DK} r_D \kappa_D \cos(\delta_B^{DK} - \delta_D)\cos\phi_3}, \\
\mathcal{A}_{\rm OS}^{DK} &= \frac{2r_B^{DK} r_D \kappa_D \sin(\delta_B^{DK} + \delta_D)\sin\phi_3}{(r_B^{DK})^2 + r_D^2 + 2r_B^{DK} r_D \kappa_D \cos(\delta_B^{DK} + \delta_D)\cos\phi_3}, \\
\mathcal{A}_{\rm SS}^{D\pi} &= \frac{2r_B^{D\pi} r_D \kappa_D \sin(\delta_B^{D\pi} - \delta_D)\sin\phi_3}{1 + (r_B^{D\pi})^2 r_D^2 + 2r_B^{D\pi} r_D \kappa_D \cos(\delta_B^{D\pi} - \delta_D)\cos\phi_3}, \\
\mathcal{A}_{\rm OS}^{D\pi} &= \frac{2r_B^{D\pi} r_D \kappa_D \sin(\delta_B^{D\pi} + \delta_D)\sin\phi_3}{(r_B^{D\pi})^2 + r_D^2 + 2r_B^{D\pi} r_D \kappa_D \cos(\delta_B^{D\pi} + \delta_D)\cos\phi_3}. \\
\mathcal{R}_{\rm SS}^{DK/D\pi} &= R\frac{1 + (r_B^{DK})^2 r_D^2 + 2r_B^{DK} r_D \kappa_D \cos(\delta_B^{DK} - \delta_D)\cos\phi_3}{1 + (r_B^{D\pi})^2 r_D^2 + 2r_B^{D\pi} r_D \kappa_D \cos(\delta_B^{D\pi} - \delta_D)\cos\phi_3}, \\
\mathcal{R}_{\rm OS}^{DK/D\pi} &= R\frac{(r_B^{DK})^2 + r_D^2 + 2r_B^{DK} r_D \kappa_D \cos(\delta_B^{DK} + \delta_D)\cos\phi_3}{(r_B^{D\pi})^2 + r_D^2 + 2r_B^{D\pi} r_D \kappa_D \cos(\delta_B^{D\pi} + \delta_D)\cos\phi_3}, \\
\mathcal{R}_{\rm SS/OS}^{D\pi} &= \frac{1 + (r_B^{D\pi})^2 r_D^2 + 2r_B^{D\pi} r_D \kappa_D \cos(\delta_B^{D\pi} - \delta_D)\cos\phi_3}{(r_B^{D\pi})^2 + r_D^2 + 2r_B^{D\pi} r_D \kappa_D \cos(\delta_B^{D\pi} + \delta_D)\cos\phi_3},
\end{aligned}
\tag{2.4}
$$

where $r_B^{DK}(r_B^{D\pi})$ is the ratio of the magnitudes of the suppressed-to-favoured amplitudes for the $B^+ \to DK^+(D\pi^+)$ decay, $\delta_B^{DK}(\delta_B^{D\pi})$ is the relative strong-phase difference between those amplitudes, r_D and δ_D are the amplitude ratio and strong-phase difference, respectively, between $D^0 \to K_{\rm S}^0 K^-\pi^+$ and $D^0 \to K_{\rm S}^0 K^+\pi^-$ decays, κ_D is the coherence factor of these D decays [10], and R is the ratio between $B^+ \to \overline{D}^0 K^+$ and $B^+ \to \overline{D}^0\pi^+$ branching fractions.

3 Belle and Belle II detectors

The Belle detector [12, 14] was a large-solid-angle magnetic spectrometer at the KEKB accelerator [15, 16], which collided 8 GeV electrons with 3.5 GeV positrons. The subdetectors of Belle most relevant for our study are the silicon vertex detector and the central drift chamber for charged-particle tracking and ionization-energy loss measurement and the aerogel threshold Cherenkov counters and time-of-flight scintillation counters for charged particle identification (PID). They were situated in a uniform axial magnetic field of 1.5 T.

The Belle II detector [13] is an upgrade of the Belle detector at the SuperKEKB accelerator [17], which collides 7 GeV electrons with 4 GeV positrons. Innermost is a tracking system, including two layers of silicon pixel sensors, four layers of silicon strip detectors, and the central drift chamber. Only 15% of the azimuthal angle is covered by the second layer of the pixel detector for the Belle II data used in this paper. Outside the drift chamber, the time-of-propagation and aerogel ring-imaging Cherenkov subdetectors cover the barrel and forward endcap regions, respectively. Outside these subdetectors are the electromagnetic calorimeter and a solenoid, which provides a uniform 1.5 T magnetic field. A $K_{\rm L}^0$ and muon detector is installed in the iron flux-return yoke of the solenoid.

JHEP09(2023)146

4 Simulation

We use simulated samples to identify sources of background, optimise selection criteria, calculate selection efficiencies, and distinguish fit models. We generate $e^+e^- \to \Upsilon(4S) \to B\overline{B}$ events, and simulate particle decays with EvtGen [18]; we generate continuum $e^+e^- \to q\overline{q}$ where q is an u, d, c, or s quark with Pythia [19] for Belle and KKMC [20] and Pythia for Belle II; we simulate final-state radiation with Photos [21]; we simulate detector response using Geant3 [22] for Belle and Geant4 [23] for Belle II. We model our signal processes using both nonresonant $D \to K^0_S K^\pm \pi^\mp$ and $D \to K^{*\mp} K^\pm$ decays. In the Belle simulation, beam backgrounds are taken into account by overlaying random trigger data. In the Belle II simulation, they are accounted for by simulating the Touschek effect [24], beam-gas scattering, and luminosity-dependent backgrounds from Bhabha scattering and two-photon quantum-electrodynamic processes [25, 26].

5 Event selection

We reconstruct events using the Belle II analysis software for both Belle and Belle II data [27–29]. All events are required to pass the online selection criteria based on either total energy deposition in the electromagnetic calorimeter or the number of charged-particle tracks in the central drift chamber. The efficiency of the online selection is found to be close to 100%.

Tracks originating from $K^\pm$ and $\pi^\pm$ are selected by requiring that each have a distance of closest approach to the e^+e^- interaction point smaller than 1.0 cm in the longitudinal direction (parallel to the e^+ beam at Belle and the principal axis of the magnet at Belle II) and smaller than 0.2 cm in the transverse plane. We identify the species of each charged hadron using $\mathcal{L}(K/\pi) = \mathcal{L}(K)/[\mathcal{L}(K) + \mathcal{L}(\pi)]$, where $\mathcal{L}(h)$ is the likelihood for hadron h to have produced the relevant track based on information from the aerogel threshold Cherenkov counters, time-of-flight scintillation counters, and the central drift chamber for Belle and all subdetectors for Belle II.

We identify an $h^\pm$ as a kaon if $\mathcal{L}(K/\pi) > 0.6$. To improve signal efficiency, no PID requirement is applied to the pion candidate from D decay. Only prompt pion candidates, which are produced directly from $B^\pm$ decay, are required to satisfy $\mathcal{L}(K/\pi) < 0.6$. In Belle II data, we also restrict the polar angle of the prompt $h^\pm$ in the laboratory frame to be within the acceptance of the PID detectors. The kaon-identification efficiency depends on the particle momentum and is in the range of 86%–90%. The rate to misidentify a pion as a kaon is in the range of 3%–9%.

We reconstruct K^0_S mesons via their decays to $\pi^+\pi^-$. Each candidate K^0_S is formed from a pair of oppositely-charged particles with no PID requirements, constrained to come from a common vertex. The resulting dipion mass must be in the range of $[487, 508]\,\mathrm{MeV}/c^2$, which corresponds to $\pm 3\sigma$ around the known K^0 mass [5], with σ being the mass resolution. To improve purity, we reject combinatorial background based on the output of a neural network for Belle [30] and a boosted decision tree (BDT) [31] for Belle II. For the latter one, 15 input variables are selected including kinematic quantities and the number of hits

JHEP09(2023)146

in the vertex detector associated to the $\pi^{\pm}$ tracks. The most discriminating variables are the angle between the directions of the K^0_S momentum and the decay position seen from the beam interaction point in the laboratory frame and the flight length of the K^0_S normalised by its uncertainty.

Each neutral D candidate, reconstructed from K^0_S, $K^{\pm}$, and $\pi^{\mp}$ candidates, must have a mass in the range of $[1.85, 1.88]\,\mathrm{GeV}/c^2$, which corresponds to $\pm 3\sigma$ around the known D^0 mass [5], where σ is the typical D mass resolution.

Each $B^{\pm}$ candidate is reconstructed from D and prompt $h^{\pm}$ candidates. To suppress continuum background, we require that the beam-constrained mass,

$$M_{\mathrm{bc}} \equiv \sqrt{s/4 - |\vec{p}_B c|^2}/c^2, \tag{5.1}$$

exceed $5.27\,\mathrm{GeV}/c^2$, where s is the squared collision energy and $\vec{p}_B$ is the B momentum, both defined in the e^+e^- centre-of-mass (c.m.) frame. We also require $|\Delta E| < 0.15\,\mathrm{GeV}$, where $\Delta E \equiv E_B - \sqrt{s}/2$ and E_B is the B energy in the c.m. frame.

The remaining background comes mostly from continuum events, which are topologically distinguishable from $B\overline{B}$ events. Since the momentum of a B is only $333\,\mathrm{MeV}/c$ in the c.m. frame, the final-state particles of a $B\overline{B}$ event are almost isotropically distributed in the c.m. frame. The final-state particles of continuum events form mainly back-to-back jets. We discriminate between $B\overline{B}$ and continuum events using modified Fox-Wolfram moments [32, 33], the thrust of the B decay products [34], the angle between the axis of this thrust and that of the particles in the rest of the event (ROE), the polar angle of the B momentum, the distance between the B decay vertex and that of the ROE in the longitudinal direction, and the output of a B-flavour-tagging algorithm [35, 36].[3] All frame-dependent quantities are calculated in the c.m. frame. Simulated samples show that these variables have correlations of 4% or smaller with ΔE, which is used in the signal-extraction fit. We train BDT classifiers with these variables separately for Belle and Belle II. The classifier output, C, is distributed between zero and one. We require $C > 0.3$, which rejects 64.3% of continuum background candidates and retains 95.3% of signal candidates for Belle and rejects 63.0% of continuum background candidates and retains 97.2% of signal candidates for Belle II.

We suppress $B^{\pm}$ candidates in which the D comes from a $D^{*\pm}$ decay by reconstructing possible $D^{*\pm}$ candidates from the D and a charged particle (assumed to be a pion) from the ROE and vetoing any $B^{\pm}$ candidate whose D forms a $D^{*\pm}$ with mass difference $M(K^0_S K^+\pi^-\pi^{\pm}) - M(K^0_S K^+\pi^-)$ in the range of $[143, 148]\,\mathrm{MeV}/c^2$.

Remaining background candidates come from continuum events, cross-feed background from signal events in which the prompt $K^{\pm}$ is misidentified as a $\pi^{\pm}$ or the reverse, or from other B decays such as $B^{\pm} \to D^* h^{\pm}$ or $B^{\pm} \to D K^{*\pm}$. Sidebands in D mass, $[1.73, 1.85]\,\mathrm{GeV}/c^2$ and $[1.88, 1.94]\,\mathrm{GeV}/c^2$, show no significant backgrounds from $B^{\pm}$ decays without intermediate D mesons.

On average, 1.02 $B^{\pm}$ candidates are reconstructed per event. In events with multiple candidates, we keep only the one with the smallest χ^2 calculated from the measured and

[3] For Belle II, a category-based algorithm is adopted.

JHEP09(2023)146

known masses of the D, $M_{\rm bc}$, the known B mass, and the resolutions on both measured masses. Simulated samples show that we select the correct candidate in 78% of such events.

6 Signal extraction

To determine the CP asymmetries and branching-fraction ratios, we fit to the two-dimensional distributions of ΔE and C', a transformation of C that is uniformly distributed between zero and one for signal and peaks at zero for continuum background [7]. We model their distributions independently since they have negligible correlations according to simulation. We perform an unbinned extended maximum-likelihood fit simultaneously in sixteen subsets of the data formed by the Cartesian product of the two charges of the $B^\pm$, the two relative charges of the $K^\pm$ from D, the two species of the prompt $h^\pm$, and the two experiments. The fit function accounts for contributions from the signal decays, continuum background, cross-feed background, and other $B\overline{B}$ backgrounds. We perform the fit separately for the full D phase space and for the $K^{*\pm}$ region.

For the signal component, we model ΔE as a sum of two Gaussian functions and an asymmetric Gaussian function with all parameters fixed to values determined from simulated samples, except for the common mean of all three Gaussian functions and a common multiplier for all their widths, which account for differences in resolution between the experiment and simulation. We model C' as uniformly distributed.

For the continuum component, we model ΔE as a straight line and C' as the sum of two exponential functions. All parameters but the slope of the line and the rate parameter for the steeper exponential are fixed to values determined from simulated samples.

For the cross-feed component, we model ΔE identically to signal, but with its own parameters, and C' as a straight line, with independent parameters for the DK and $D\pi$ data and all parameters fixed to values determined from simulated samples.

For the $B\overline{B}$-background component, we model ΔE as a sum of two exponential functions and C' as a straight line, with independent parameters for DK and $D\pi$ and all parameters except for the rate parameter of the steeper exponential function fixed to values determined from simulated samples.

For each data subset i, the total number of events $n^{Dh^\pm}_{{\rm tot},i}$ with no PID requirement are related to the observed numbers of signal events $n^{Dh^\pm}_{{\rm sig},i}$, cross-feed background yields $n^{Dh^\pm}_{{\rm bkg},i}$, and the PID efficiencies $\epsilon_{h^\pm}$ as follows:

$$n^{DK^\pm}_{{\rm sig},i} = \epsilon_{K^\pm} n^{DK^\pm}_{{\rm tot},i}\,, \tag{6.1}$$

$$n^{D\pi^\pm}_{{\rm sig},i} = \epsilon_{\pi^\pm} n^{D\pi^\pm}_{{\rm tot},i}\,, \tag{6.2}$$

$$n^{DK^\pm}_{{\rm bkg},i} = (1-\epsilon_{\pi^\pm}) n^{D\pi^\pm}_{{\rm tot},i}\,, \tag{6.3}$$

$$n^{D\pi^\pm}_{{\rm bkg},i} = (1-\epsilon_{K^\pm}) n^{DK^\pm}_{{\rm tot},i}\,. \tag{6.4}$$

In the fit, the $n^{DK^\pm}_{{\rm tot},i}$ and $n^{D\pi^\pm}_{{\rm tot},i}$ yields are expressed in terms of the CP asymmetries and branching-fraction ratios, the sum of all $n^{D\pi}_{{\rm tot},i}$, and the ratio δ of the efficiency for detecting $B^\pm \to DK^\pm$ over that for $B^\pm \to D\pi^\pm$ decays. The PID efficiencies and δ are fixed from simulated samples and corrected for discrepancies between experiment and simulation

JHEP09(2023)146

	Belle	Belle II
ϵ_{K^+}	0.845 ± 0.009	0.820 ± 0.005
ϵ_{K^-}	0.853 ± 0.008	0.821 ± 0.004
ϵ_{π^+}	0.926 ± 0.008	0.929 ± 0.003
ϵ_{π^-}	0.930 ± 0.009	0.918 ± 0.003
δ	0.973 ± 0.005	0.972 ± 0.004

Table 1. PID and tracking efficiencies.

that depend on particle momentum, direction, charge, and species. Those corrections range between 0.960 and 0.984, with typical uncertainties of 0.008 to 0.009, as estimated using the control channels $D^{*+} \to D^0(\to K^-\pi^+)\pi^+$, and $K^0_S \to \pi^+\pi^-$ for $K^\pm$ and $\pi^\pm$. Table 1 lists the post-correction efficiencies and δ with uncertainties including those on the corrections. We validate the fit strategy using simplified simulated experiments and find unbiased estimates and Gaussian uncertainties for all parameters of interest.

The fits determine the sums of all $n^{D\pi}_{\text{tot},i}$ yields in the full D phase space to be 2209 ± 59 for Belle and 1210 ± 39 for Belle II and in the region of the $K^{*\pm}$ to be 1337 ± 42 for Belle and 732 ± 30 for Belle II. The sum of all $n^{DK}_{\text{tot},i}$ yields is calculated using the fit results, and is 238 ± 21 for Belle and 131 ± 12 for Belle II for the full D phase space and 126 ± 15 for Belle and 69 ± 9 for Belle II in the region of the $K^{*\pm}$. Figures 1–4 show the data and fit results for the full D phase space and figures 5–8 show the same distributions for the $K^{*\pm}$ region. We enhance the signal in the plots by displaying ΔE distributions for events with $C' > 0.6$ and C' distributions for events with $|\Delta E| < 0.05\,\text{GeV}$. In the ΔE distributions of the DK data subset, the cross-feed component from $D\pi$ is visible as a peak at higher ΔE values.

7 Systematic uncertainties

We consider the sources of systematic uncertainties listed in table 2. For the first three sources in the table, we estimate the systematic effects associated with the fixed efficiencies in the fit and the uncertainties in the choice of model parameters. We vary the values for the fixed parameters one thousand times, sampling them from a multivariate Gaussian distribution with the known uncertainties and correlations. We repeat the fit for each variation and inspect the distributions of results. If they are approximately Gaussian, we take the standard deviations as systematic uncertainties. If they are non-Gaussian, we conservatively take the full ranges of the distributions as the systematic uncertainties. For the ΔE shape of the continuum component, which does not have any fixed parameters, we repeat the fit using a second-order polynomial function as an alternative model and take the changes of the fit results as systematic uncertainties.

In our fits, we assume equal efficiencies for detecting and reconstructing $D \to K^0_S K^-\pi^+$ and $D \to K^0_S K^+\pi^-$ decays. In simulation, the ratio of the former to the latter is 0.98. We repeat the analysis using this value and assign the differences in the results as systematic uncertainties. Our simulated samples are generated assuming the D decay products are evenly

JHEP09(2023)146

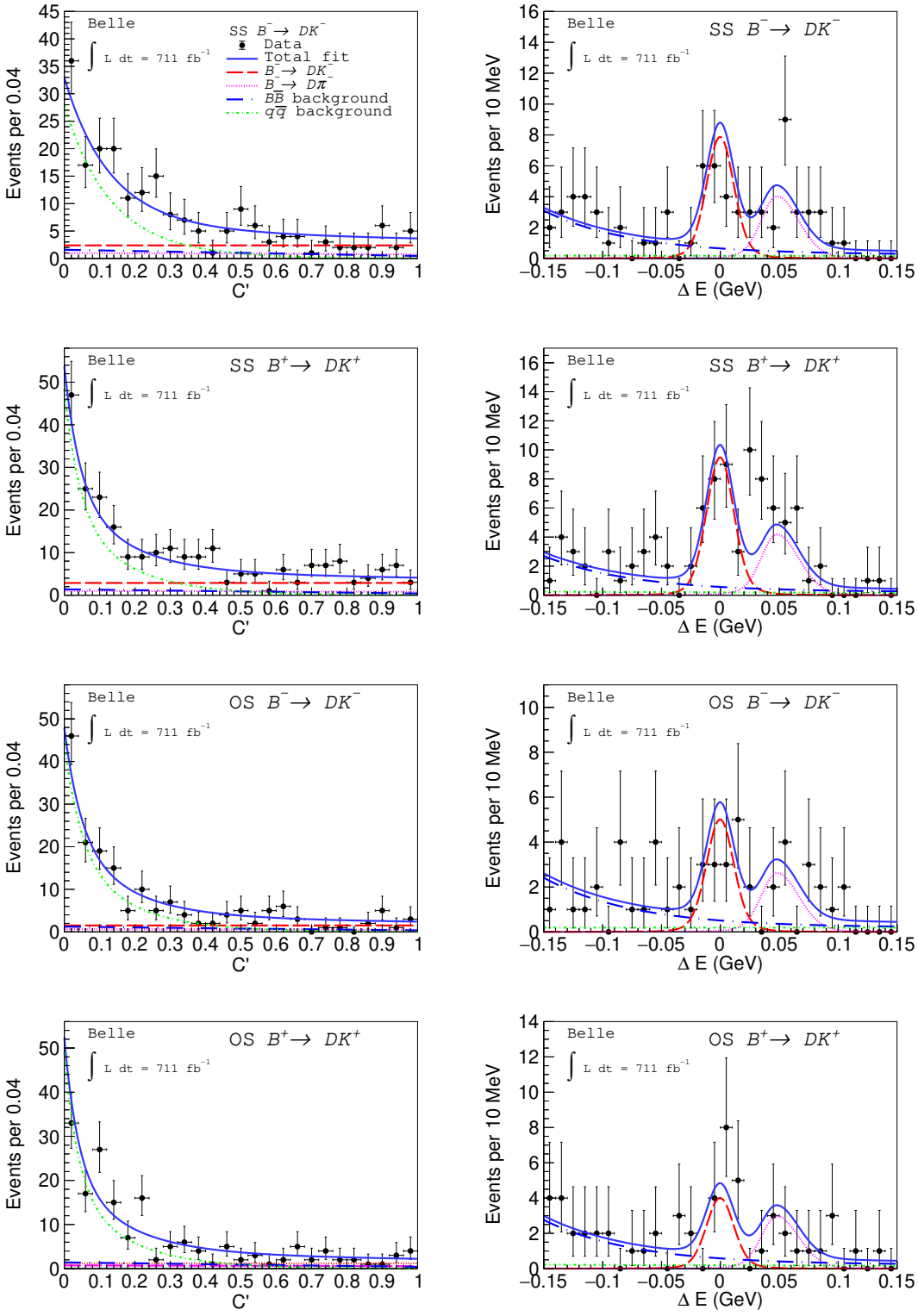

Figure 1. Distributions of C' and ΔE for $B^{\pm} \to DK^{\pm}$ candidates reconstructed in the Belle data for the full D phase space, with the fit results overlaid. The SS or OS indicates the type of the signal decay chain, same-sign or opposite-sign, respectively.

JHEP09(2023)146

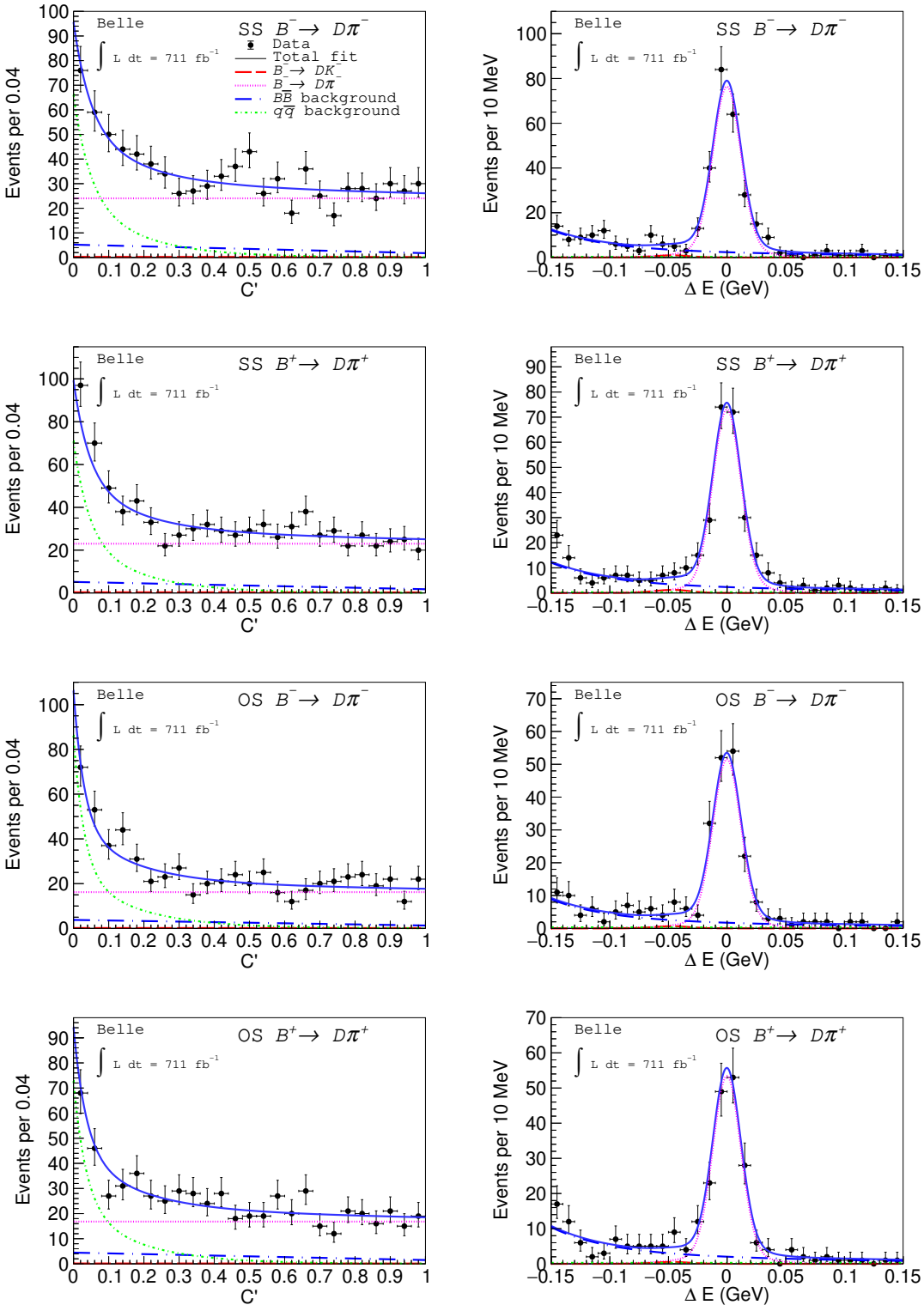

Figure 2. Distributions of C' and ΔE for $B^\pm \to D\pi^\pm$ candidates reconstructed in the Belle data for the full D phase space, with the fit results overlaid. The SS or OS indicates the type of the signal decay chain, same-sign or opposite-sign, respectively.

JHEP09(2023)146

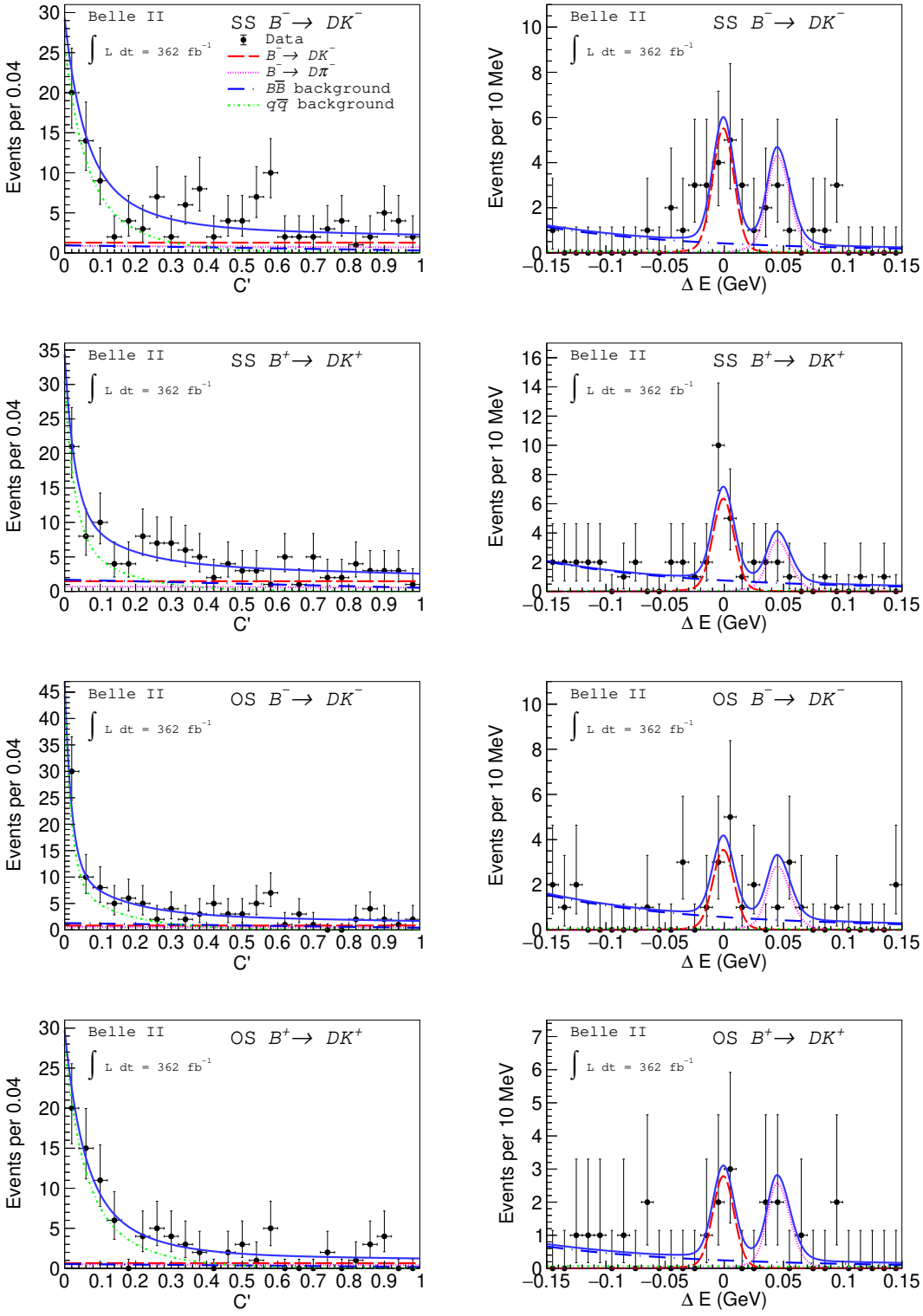

Figure 3. Distributions of C' and ΔE for $B^\pm \to DK^\pm$ candidates reconstructed in the Belle II data for the full D phase space, with the fit results overlaid. The SS or OS indicates the type of the signal decay chain, same-sign or opposite-sign, respectively.

JHEP09(2023)146

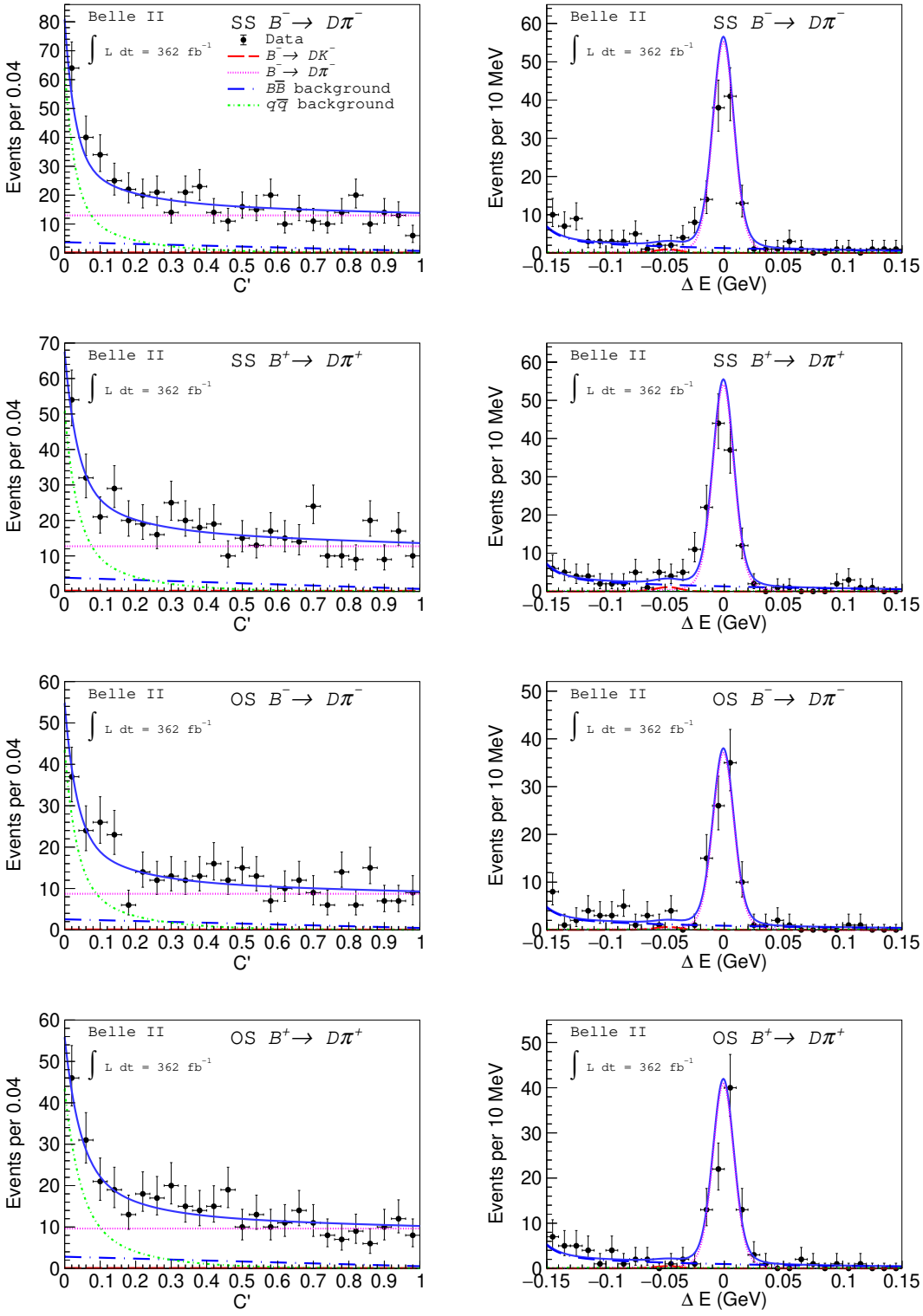

Figure 4. Distributions of C' and ΔE for $B^\pm \to D\pi^\pm$ candidates reconstructed in the Belle II data for the full D phase space, with the fit results overlaid. The SS or OS indicates the type of the signal decay chain, same-sign or opposite-sign, respectively.

JHEP09(2023)146

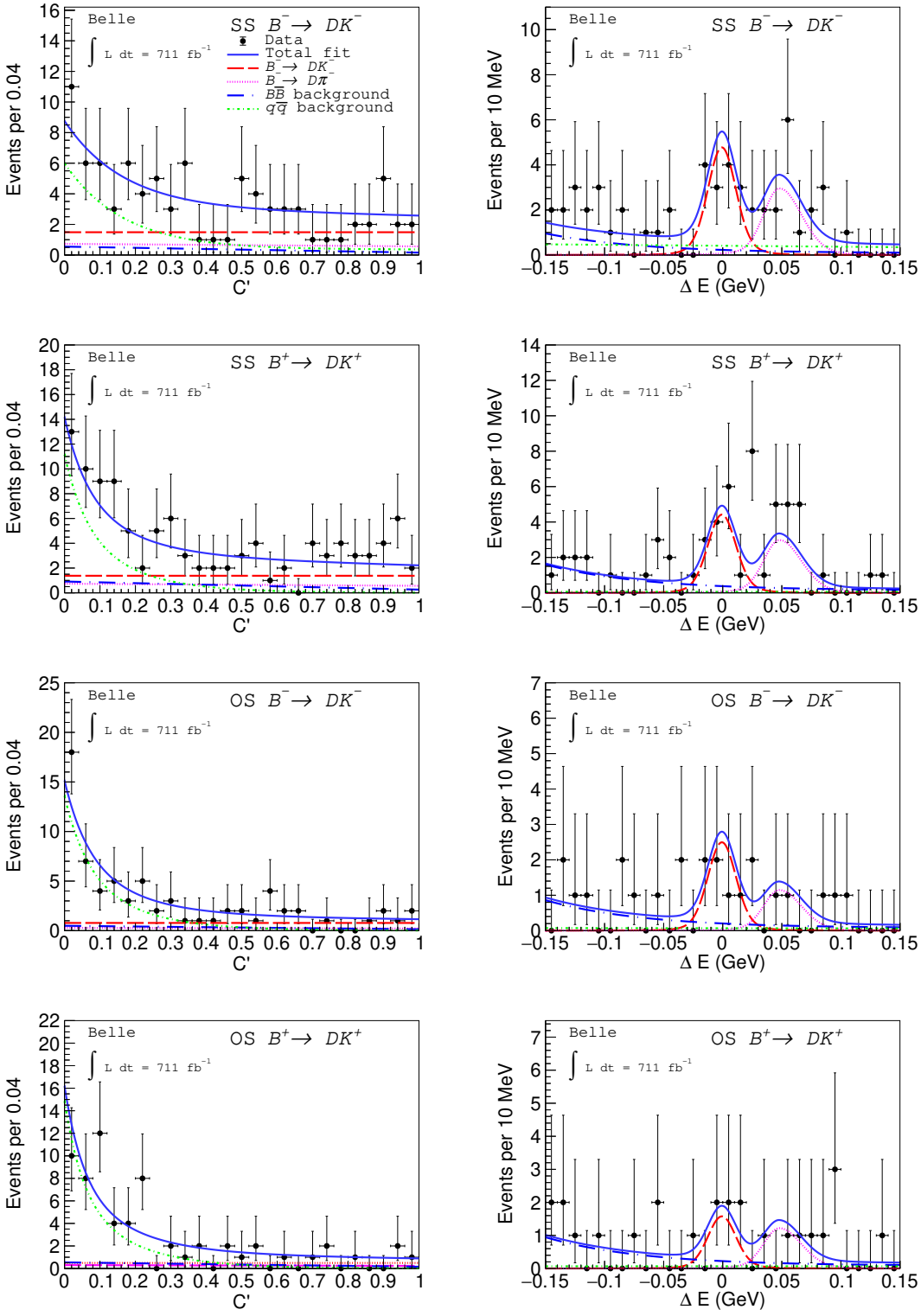

Figure 5. Distributions of C' and ΔE for $B^{\pm} \to DK^{\pm}$ candidates reconstructed in the Belle data for the $K^{*\pm}$ region, with the fit results overlaid. The SS or OS indicates the type of the signal decay chain, same-sign or opposite-sign, respectively.

JHEP09(2023)146

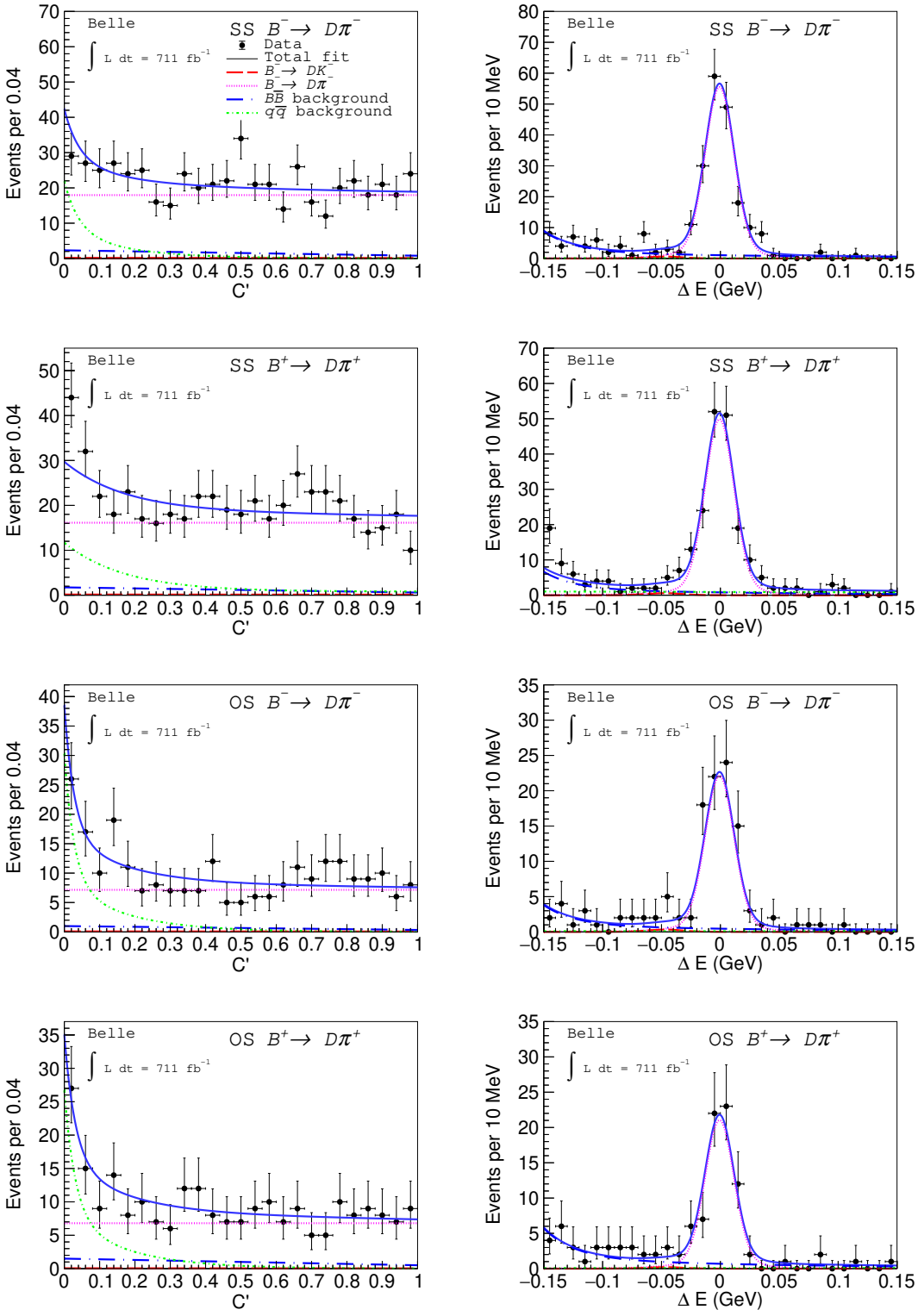

Figure 6. Distributions of C' and ΔE for $B^\pm \to D\pi^\pm$ candidates reconstructed in the Belle data for the $K^{*\pm}$ region, with the fit results overlaid. The SS or OS indicates the type of the signal decay chain, same-sign or opposite-sign, respectively.

JHEP09(2023)146

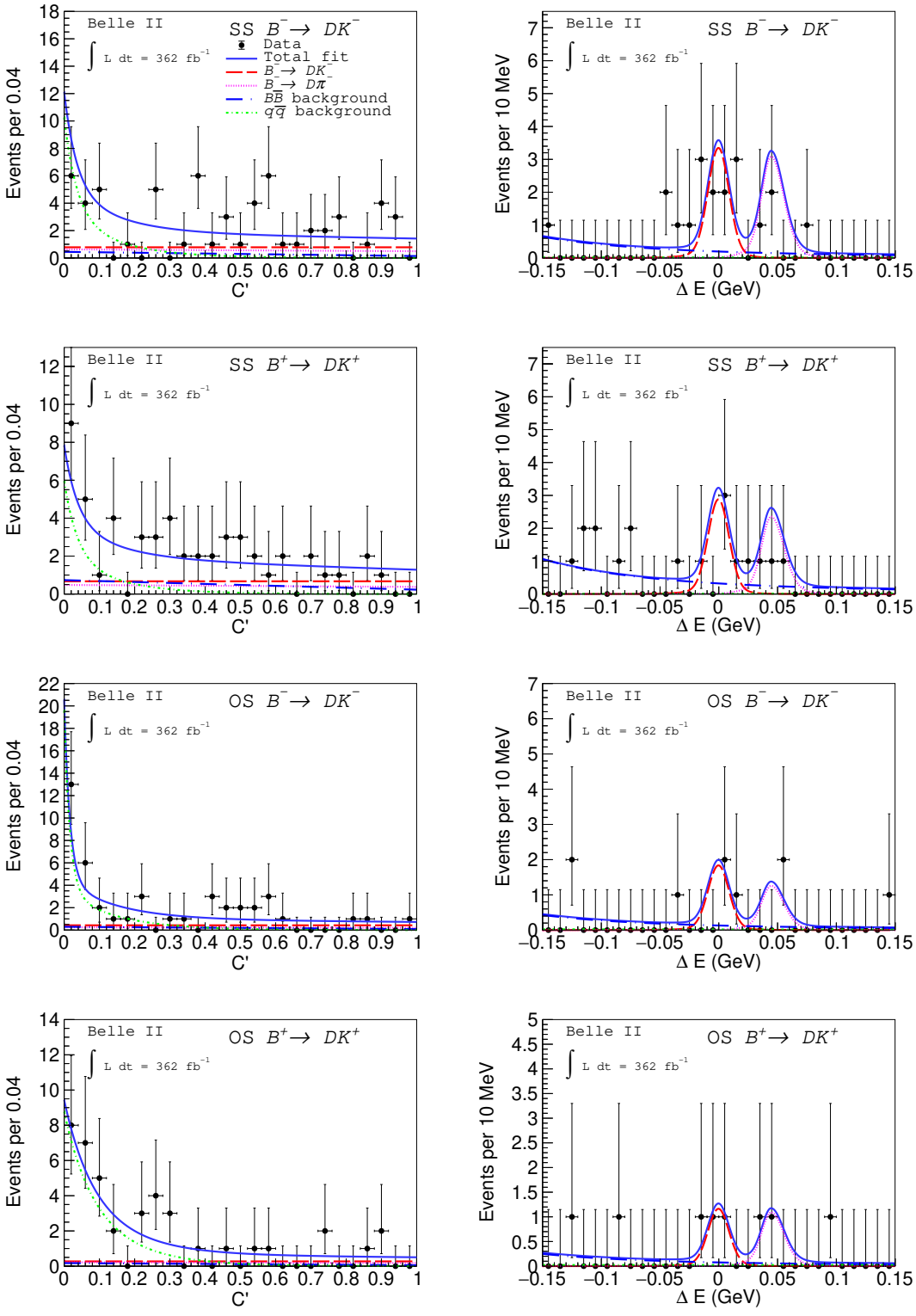

Figure 7. Distributions of C' and ΔE for $B^\pm \to DK^\pm$ candidates reconstructed in the Belle II data for the $K^{*\pm}$ region, with the fit results overlaid. The SS or OS indicates the type of the signal decay chain, same-sign or opposite-sign, respectively.

JHEP09(2023)146

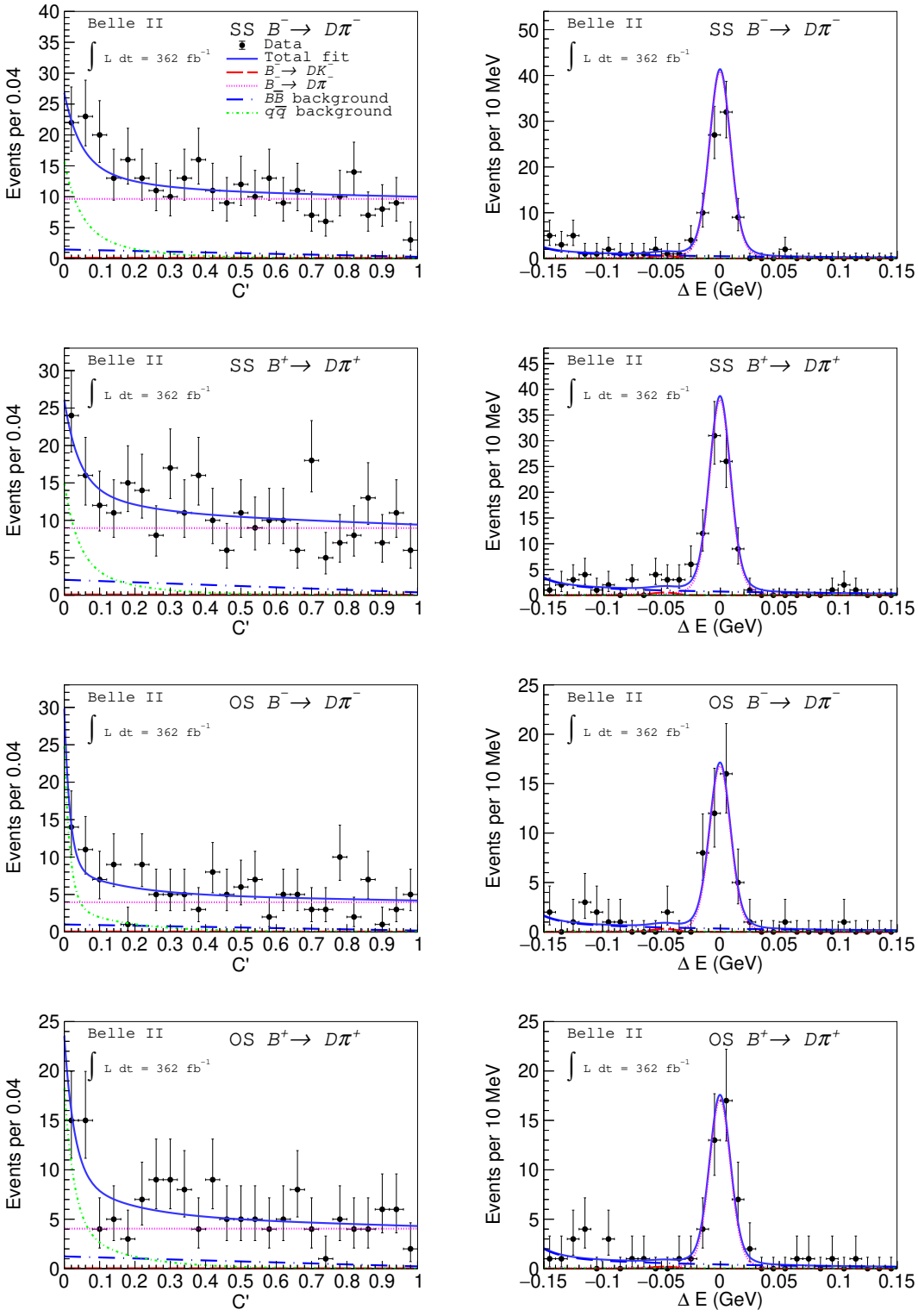

Figure 8. Distributions of C' and ΔE for $B^\pm \to D\pi^\pm$ candidates reconstructed in the Belle II data for the $K^{*\pm}$ region, with the fit results overlaid. The SS or OS indicates the type of the signal decay chain, same-sign or opposite-sign, respectively.

JHEP09(2023)146

	$A_{\rm SS}^{DK}$	$A_{\rm OS}^{DK}$	$A_{\rm SS}^{D\pi}$	$A_{\rm OS}^{D\pi}$	$R_{\rm SS}^{DK/D\pi}$	$R_{\rm OS}^{DK/D\pi}$	$R_{\rm SS/OS}^{D\pi}$
Full D phase space							
$\epsilon_{K^\pm}, \epsilon_{\pi^\pm}$	0.38	0.56	0.19	0.14	0.05	0.06	0.09
δ	—	0.03	—	—	0.04	0.03	0.02
Model	0.62	0.78	0.02	0.02	0.30	0.22	0.07
$\epsilon_{K^0_S K^-\pi^+}/\epsilon_{K^0_S K^+\pi^-}$	0.82	0.83	0.82	0.83	0.01	0.01	0.02
Total syst. unc.	1.1	1.3	0.9	0.9	0.4	0.3	0.2
Stat. unc.	9.1	13.3	2.6	3.1	1.2	1.3	5.7
$K^{*\pm}$ region							
$\epsilon_{K^\pm}, \epsilon_{\pi^\pm}$	0.37	0.61	0.17	0.15	0.03	0.08	0.13
δ	0.02	0.02	0.01	0.01	0.03	0.04	0.04
Model	1.04	0.97	0.20	0.03	0.46	0.49	0.61
$\epsilon_{K^0_S K^-\pi^+}/\epsilon_{K^0_S K^+\pi^-}$	1.6	0.8	1.6	0.8	0.1	0.1	1.7
Total syst. unc.	2.0	1.4	1.6	0.9	0.5	0.6	1.9
Stat. unc.	11.9	18.4	2.9	4.6	1.2	2.0	13.2

Table 2. Systematic and statistical uncertainties in units of 10^{-2}. The entries "—" indicate uncertainties smaller than 10^{-4}.

distributed in the available phase space, which is not the distribution expected in the data. However, the efficiency ratios calculated with an alternative decay model of $D \to K^{*\pm}K^{\mp}$, which is the dominant process in $D \to K^0_S K^{\mp}\pi^{\pm}$ [5], are equivalent to the nominal ones.

8 Results

The results from the Belle and Belle II data for the full D phase space are

$$A_{\rm SS}^{DK} = -0.089 \pm 0.091 \pm 0.011, \tag{8.1}$$
$$A_{\rm OS}^{DK} = 0.109 \pm 0.133 \pm 0.013, \tag{8.2}$$
$$A_{\rm SS}^{D\pi} = 0.018 \pm 0.026 \pm 0.009, \tag{8.3}$$
$$A_{\rm OS}^{D\pi} = -0.028 \pm 0.031 \pm 0.009, \tag{8.4}$$
$$R_{\rm SS}^{DK/D\pi} = 0.122 \pm 0.012 \pm 0.004, \tag{8.5}$$
$$R_{\rm OS}^{DK/D\pi} = 0.093 \pm 0.013 \pm 0.003, \tag{8.6}$$
$$R_{\rm SS/OS}^{D\pi} = 1.428 \pm 0.057 \pm 0.002, \tag{8.7}$$

JHEP09(2023)146

	$A_{\rm OS}^{DK}$	$A_{\rm SS}^{D\pi}$	$A_{\rm OS}^{D\pi}$	$R_{\rm SS}^{DK/D\pi}$	$R_{\rm OS}^{DK/D\pi}$	$R_{\rm SS/OS}^{D\pi}$
$A_{\rm SS}^{DK}$	0.001	−0.010	0.000	0.001	−0.000	0.003
$A_{\rm OS}^{DK}$		0.000	−0.006	0.003	0.008	−0.001
$A_{\rm SS}^{D\pi}$			0.000	0.006	−0.001	−0.004
$A_{\rm OS}^{D\pi}$				0.001	0.001	0.001
$R_{\rm SS}^{DK/D\pi}$					0.038	−0.176
$R_{\rm OS}^{DK/D\pi}$						0.178

Table 3. Statistical correlations for results in the full D phase space using Belle and Belle II data.

and for the $K^{*\pm}$ region are

$$A_{\rm SS}^{DK} = 0.055 \pm 0.119 \pm 0.020, \tag{8.8}$$
$$A_{\rm OS}^{DK} = 0.231 \pm 0.184 \pm 0.014, \tag{8.9}$$
$$A_{\rm SS}^{D\pi} = 0.046 \pm 0.029 \pm 0.016, \tag{8.10}$$
$$A_{\rm OS}^{D\pi} = 0.009 \pm 0.046 \pm 0.009, \tag{8.11}$$
$$R_{\rm SS}^{DK/D\pi} = 0.093 \pm 0.012 \pm 0.005, \tag{8.12}$$
$$R_{\rm OS}^{DK/D\pi} = 0.103 \pm 0.020 \pm 0.006, \tag{8.13}$$
$$R_{\rm SS/OS}^{D\pi} = 2.412 \pm 0.132 \pm 0.019, \tag{8.14}$$

where the first uncertainty is statistical and the second is systematic. Tables 3–6 list the statistical and systematic correlations of all results. Our results are consistent with LHCb's results [11], with worse precision due to a smaller sample size. This study is also performed with the Belle data set alone and the results are reported in appendix A.

Our results alone do not allow for an unambiguous determination of ϕ_3, but combined with other results in global fits they constrain it. The enhancement of the $D \to K_{\rm S}^0 K^\pm \pi^\mp$'s coherence factor κ_D in the $K^{*\pm}$ region indicated by the current CLEO measurement [10] suggests the possibility of an enhancement of the CP-violating asymmetry in that region. However, the current precisions of both GLS results from this paper and strong-phase difference results prevent a conclusive statement if such enhancement is sufficient to compensate for the extra efficiency loss due to the phase space restriction.

9 Summary

We measure the CP asymmetries and branching-fraction ratios for $B^\pm \to DK^\pm$ and $B^\pm \to D\pi^\pm$ decays with $D \to K_{\rm S}^0 K^\pm \pi^\mp$ using the full Belle data set containing 772×10^6 $B\overline{B}$ pairs and a Belle II data set containing 387×10^6 $B\overline{B}$ pairs. We extract these observables simultaneously through a simultaneous fit across data sets and channels for the full D phase space and in the region of the $K^{*\pm}$. These results, combined with other ϕ_3-related results, constrain the unitarity triangle angle ϕ_3.

JHEP09(2023)146

	$A_{\rm OS}^{DK}$	$A_{\rm SS}^{D\pi}$	$A_{\rm OS}^{D\pi}$	$R_{\rm SS}^{DK/D\pi}$	$R_{\rm OS}^{DK/D\pi}$	$R_{\rm SS/OS}^{D\pi}$
$A_{SS,DK}$	0.390	−0.002	0.065	0.409	0.447	0.129
$A_{OS,DK}$		0.025	0.001	0.205	0.234	0.032
$A_{SS,D\pi}$			0.036	0.052	0.043	−0.048
$A_{OS,D\pi}$				0.094	0.086	0.063
$R_{SS,DK/D\pi}$					0.953	−0.072
$R_{OS,DK/D\pi}$						0.089

Table 4. Systematic correlations for results in the full D phase space using Belle and Belle II data.

	$A_{\rm OS}^{DK}$	$A_{\rm SS}^{D\pi}$	$A_{\rm OS}^{D\pi}$	$R_{\rm SS}^{DK/D\pi}$	$R_{\rm OS}^{DK/D\pi}$	$R_{\rm SS/OS}^{D\pi}$
$A_{\rm SS}^{DK}$	0.003	−0.012	0.001	−0.052	−0.013	0.002
$A_{\rm OS}^{DK}$		0.001	−0.011	−0.004	−0.034	0.002
$A_{\rm SS}^{D\pi}$			0.000	0.002	−0.004	−0.011
$A_{\rm OS}^{D\pi}$				−0.002	−0.002	0.014
$R_{\rm SS}^{DK/D\pi}$					0.034	−0.132
$R_{\rm OS}^{DK/D\pi}$						0.208

Table 5. Statistical correlations for results in the region of the $K^{*\pm}$ using Belle and Belle II data.

	$A_{\rm OS}^{DK}$	$A_{\rm SS}^{D\pi}$	$A_{\rm OS}^{D\pi}$	$R_{\rm SS}^{DK/D\pi}$	$R_{\rm OS}^{DK/D\pi}$	$R_{\rm SS/OS}^{D\pi}$
$A_{SS,DK}$	0.195	0.046	0.013	0.120	−0.053	0.191
$A_{OS,DK}$		0.038	0.004	0.344	0.210	0.006
$A_{SS,D\pi}$			0.023	−0.004	−0.037	0.017
$A_{OS,D\pi}$				−0.016	−0.023	0.006
$R_{SS,DK/D\pi}$					0.914	0.015
$R_{OS,DK/D\pi}$						−0.097

Table 6. Systematic correlations for results in the region of the $K^{*\pm}$ using Belle and Belle II data.

JHEP09(2023)146

	$A_{\rm OS}^{DK}$	$A_{\rm SS}^{D\pi}$	$A_{\rm OS}^{D\pi}$	$R_{\rm SS}^{DK/D\pi}$	$R_{\rm OS}^{DK/D\pi}$	$R_{\rm SS/OS}^{D\pi}$
$A_{\rm SS}^{DK}$	0.000	−0.015	0.000	0.027	0.002	0.004
$A_{\rm OS}^{DK}$		−0.000	−0.013	0.004	0.051	0.000
$A_{\rm SS}^{D\pi}$			0.000	0.009	−0.003	−0.008
$A_{\rm OS}^{D\pi}$				−0.002	−0.000	0.007
$R_{\rm SS}^{DK/D\pi}$					0.048	−0.166
$R_{\rm OS}^{DK/D\pi}$						0.168

Table 7. Statistical correlations for results in the full D phase space using Belle data alone.

A Belle data results

The results using only Belle data for the full D phase space are

$$A_{\rm SS}^{DK} = -0.121 \pm 0.120 \pm 0.013, \tag{A.1}$$
$$A_{\rm OS}^{DK} = -0.016 \pm 0.182 \pm 0.014, \tag{A.2}$$
$$A_{\rm SS}^{D\pi} = 0.014 \pm 0.032 \pm 0.011, \tag{A.3}$$
$$A_{\rm OS}^{D\pi} = 0.001 \pm 0.039 \pm 0.011, \tag{A.4}$$
$$R_{\rm SS}^{DK/D\pi} = 0.112 \pm 0.014 \pm 0.002, \tag{A.5}$$
$$R_{\rm OS}^{DK/D\pi} = 0.085 \pm 0.016 \pm 0.002, \tag{A.6}$$
$$R_{\rm SS/OS}^{D\pi} = 1.472 \pm 0.074 \pm 0.002, \tag{A.7}$$

and for the $K^{*\pm}$ region are

$$A_{\rm SS}^{DK} = 0.028 \pm 0.163 \pm 0.022, \tag{A.8}$$
$$A_{\rm OS}^{DK} = 0.220 \pm 0.245 \pm 0.014, \tag{A.9}$$
$$A_{\rm SS}^{D\pi} = 0.041 \pm 0.036 \pm 0.011, \tag{A.10}$$
$$A_{\rm OS}^{D\pi} = 0.041 \pm 0.059 \pm 0.011, \tag{A.11}$$
$$R_{\rm SS}^{DK/D\pi} = 0.082 \pm 0.014 \pm 0.002, \tag{A.12}$$
$$R_{\rm OS}^{DK/D\pi} = 0.097 \pm 0.027 \pm 0.002, \tag{A.13}$$
$$R_{\rm SS/OS}^{D\pi} = 2.592 \pm 0.180 \pm 0.005. \tag{A.14}$$

Tables 7–10 list the statistical and systematic correlations. These results on Belle data only are provided to facilitate combinations with future updates of Belle II results.

Acknowledgments

This work, based on data collected using the Belle II detector, which was built and commissioned prior to March 2019, was supported by Science Committee of the Republic of Armenia Grant No. 20TTCG-1C010; Australian Research Council and research Grants No. DP200101792, No. DP210101900, No. DP210102831, No. DE220100462,

JHEP09(2023)146

	$A_{\rm OS}^{DK}$	$A_{\rm SS}^{D\pi}$	$A_{\rm OS}^{D\pi}$	$R_{\rm SS}^{DK/D\pi}$	$R_{\rm OS}^{DK/D\pi}$	$R_{\rm SS/OS}^{D\pi}$
$A_{SS,DK}$	0.326	−0.015	−0.073	−0.179	0.026	0.298
$A_{OS,DK}$		0.025	−0.053	−0.125	0.065	0.163
$A_{SS,D\pi}$			0.058	0.083	0.059	−0.022
$A_{OS,D\pi}$				0.036	−0.026	−0.060
$R_{SS,DK/D\pi}$					0.804	−0.313
$R_{OS,DK/D\pi}$						0.183

Table 8. Systematic correlations for results in the full D phase space using Belle data alone.

	$A_{\rm OS}^{DK}$	$A_{\rm SS}^{D\pi}$	$A_{\rm OS}^{D\pi}$	$R_{\rm SS}^{DK/D\pi}$	$R_{\rm OS}^{DK/D\pi}$	$R_{\rm SS/OS}^{D\pi}$
$A_{SS,DK}$	−0.003	−0.013	−0.001	−0.072	0.014	−0.001
$A_{OS,DK}$		−0.000	−0.021	−0.006	−0.019	0.003
$A_{SS,D\pi}$			0.000	0.005	0.001	−0.009
$A_{OS,D\pi}$				−0.002	−0.006	0.020
$R_{SS,DK/D\pi}$					0.036	−0.121
$R_{OS,DK/D\pi}$						0.196

Table 9. Statistical correlations for results in the region of the $K^{*\pm}$ using Belle data alone.

	$A_{\rm OS}^{DK}$	$A_{\rm SS}^{D\pi}$	$A_{\rm OS}^{D\pi}$	$R_{\rm SS}^{DK/D\pi}$	$R_{\rm OS}^{DK/D\pi}$	$R_{\rm SS/OS}^{D\pi}$
$A_{\rm SS}^{DK}$	0.197	0.176	−0.049	0.299	0.007	0.283
$A_{\rm OS}^{DK}$		0.056	−0.025	0.051	0.152	0.070
$A_{\rm SS}^{D\pi}$			0.056	0.035	−0.002	0.126
$A_{\rm OS}^{D\pi}$				0.009	−0.049	0.059
$R_{\rm SS}^{DK/D\pi}$					0.583	0.313
$R_{\rm OS}^{DK/D\pi}$						−0.059

Table 10. Systematic correlations for results in the region of the $K^{*\pm}$ using Belle data alone.

No. LE210100098, and No. LE230100085; Austrian Federal Ministry of Education, Science and Research, Austrian Science Fund No. P 31361-N36 and No. J4625-N, and Horizon 2020 ERC Starting Grant No. 947006 "InterLeptons"; Natural Sciences and Engineering Research Council of Canada, Compute Canada and CANARIE; National Key R&D Program of China under Contract No. 2022YFA1601903, National Natural Science Foundation of China and research Grants No. 11575017, No. 11761141009, No. 11705209, No. 11975076, No. 12135005, No. 12150004, No. 12161141008, and No. 12175041, and Shandong Provincial Natural Science Foundation Project ZR2022JQ02; the Ministry of Education, Youth, and Sports of the Czech Republic under Contract No. LTT17020 and Charles University Grant No. SVV 260448 and the Czech Science Foundation Grant No. 22-18469S; Euro-

JHEP09(2023)146

pean Research Council, Seventh Framework PIEF-GA-2013-622527, Horizon 2020 ERC-Advanced Grants No. 267104 and No. 884719, Horizon 2020 ERC-Consolidator Grant No. 819127, Horizon 2020 Marie Sklodowska-Curie Grant Agreement No. 700525 "NIOBE" and No. 101026516, and Horizon 2020 Marie Sklodowska-Curie RISE project JENNIFER2 Grant Agreement No. 822070 (European grants); L'Institut National de Physique Nucléaire et de Physique des Particules (IN2P3) du CNRS (France); BMBF, DFG, HGF, MPG, and AvH Foundation (Germany); Department of Atomic Energy under Project Identification No. RTI 4002 and Department of Science and Technology (India); Israel Science Foundation Grant No. 2476/17, U.S.-Israel Binational Science Foundation Grant No. 2016113, and Israel Ministry of Science Grant No. 3-16543; Istituto Nazionale di Fisica Nucleare and the research grants BELLE2; Japan Society for the Promotion of Science, Grant-in-Aid for Scientific Research Grants No. 16H03968, No. 16H03993, No. 16H06492, No. 16K05323, No. 17H01133, No. 17H05405, No. 18K03621, No. 18H03710, No. 18H05226, No. 19H00682, No. 22H00144, No. 26220706, and No. 26400255, the National Institute of Informatics, and Science Information NETwork 5 (SINET5), and the Ministry of Education, Culture, Sports, Science, and Technology (MEXT) of Japan; National Research Foundation (NRF) of Korea Grants No. 2016R1D1A1B02012900, No. 2018R1A2B3003643, No. 2018R1-A6A1A06024970, No. 2018R1D1A1B07047294, No. 2019R1I1A3A01058933, No. 2022R1-A2C1003993, and No. RS-2022-00197659, Radiation Science Research Institute, Foreign Large-size Research Facility Application Supporting project, the Global Science Experimental Data Hub Center of the Korea Institute of Science and Technology Information and KREONET/GLORIAD; Universiti Malaya RU grant, Akademi Sains Malaysia, and Ministry of Education Malaysia; Frontiers of Science Program Contracts No. FOINS-296, No. CB-221329, No. CB-236394, No. CB-254409, and No. CB-180023, and No. SEP-CINVESTAV research Grant No. 237 (Mexico); the Polish Ministry of Science and Higher Education and the National Science Center; the Ministry of Science and Higher Education of the Russian Federation, Agreement No. 14.W03.31.0026, and the HSE University Basic Research Program, Moscow; University of Tabuk research Grants No. S-0256-1438 and No. S-0280-1439 (Saudi Arabia); Slovenian Research Agency and research Grants No. J1-9124 and No. P1-0135; Agencia Estatal de Investigacion, Spain Grant No. RYC2020-029875-I and Generalitat Valenciana, Spain Grant No. CIDEGENT/2018/020 Ministry of Science and Technology and research Grants No. MOST106-2112-M-002-005-MY3 and No. MOST107-2119-M-002-035-MY3, and the Ministry of Education (Taiwan); Thailand Center of Excellence in Physics; TUBITAK ULAKBIM (Turkey); National Research Foundation of Ukraine, project No. 2020.02/0257, and Ministry of Education and Science of Ukraine; the U.S. National Science Foundation and research Grants No. PHY-1913789 and No. PHY-2111604, and the U.S. Department of Energy and research Awards No. DE-AC06-76RLO1830, No. DE-SC0007983, No. DE-SC0009824, No. DE-SC0009973, No. DE-SC0010007, No. DE-SC0010073, No. DE-SC0010118, No. DE-SC0010504, No. DE-SC0011784, No. DE-SC0012704, No. DE-SC0019230, No. DE-SC0021274, No. DE-SC0022350, No. DE-SC0023470; and the Vietnam Academy of Science and Technology (VAST) under Grant No. DL0000.05/21-23.

These acknowledgements are not to be interpreted as an endorsement of any statement made by any of our institutes, funding agencies, governments, or their representatives.

JHEP09(2023)146

We thank the SuperKEKB team for delivering high-luminosity collisions; the KEK cryogenics group for the efficient operation of the detector solenoid magnet; the KEK computer group and the NII for on-site computing support and SINET6 network support; and the raw-data centers at BNL, DESY, GridKa, IN2P3, INFN, and the University of Victoria for offsite computing support.

References

[1] N. Cabibbo, *Unitary symmetry and leptonic decays*, *Phys. Rev. Lett.* **10** (1963) 531 [INSPIRE].

[2] M. Kobayashi and T. Maskawa, *CP violation in the renormalizable theory of weak interaction*, *Prog. Theor. Phys.* **49** (1973) 652 [INSPIRE].

[3] J. Brod, A. Lenz, G. Tetlalmatzi-Xolocotzi and M. Wiebusch, *New physics effects in tree-level decays and the precision in the determination of the quark mixing angle γ*, *Phys. Rev. D* **92** (2015) 033002 [arXiv:1412.1446] [INSPIRE].

[4] J. Brod and J. Zupan, *The ultimate theoretical error on γ from $B \to DK$ decays*, *JHEP* **01** (2014) 051 [arXiv:1308.5663] [INSPIRE].

[5] Particle Data Group collaboration, *Review of particle physics*, *PTEP* **2022** (2022) 083C01 [INSPIRE].

[6] BaBar collaboration, *Observation of direct CP violation in the measurement of the Cabibbo-Kobayashi-Maskawa angle gamma with $B^\pm \to D^{(*)}K^{(*)\pm}$ decays*, *Phys. Rev. D* **87** (2013) 052015 [arXiv:1301.1029] [INSPIRE].

[7] Belle and Belle-II collaborations, *Combined analysis of Belle and Belle II data to determine the CKM angle ϕ_3 using $B^+ \to D(K^0_S h^- h^+)h^+$ decays*, *JHEP* **02** (2022) 063 [*Erratum ibid.* **12** (2022) 034] [arXiv:2110.12125] [INSPIRE].

[8] J.F. Klamka, *Pair production of charged IDM scalars at high energy CLIC*, *PoS* **ICHEP2022** (2022) 164.

[9] Y. Grossman, Z. Ligeti and A. Soffer, *Measuring γ in $B^\pm \to K^\pm(KK^*)_D$ decays*, *Phys. Rev. D* **67** (2003) 071301 [hep-ph/0210433] [INSPIRE].

[10] CLEO collaboration, *Studies of the decays $D^0 \to K^0_S K^-\pi^+$ and $D^0 \to K^0_S K^+\pi^-$*, *Phys. Rev. D* **85** (2012) 092016 [*Erratum ibid.* **94** (2016) 099905] [arXiv:1203.3804] [INSPIRE].

[11] LHCb collaboration, *Measurement of CP observables in $B^\pm \to DK^\pm$ and $B^\pm \to D\pi^\pm$ with $D \to K^0_S K^\pm\pi^\mp$ decays*, *JHEP* **06** (2020) 058 [arXiv:2002.08858] [INSPIRE].

[12] Belle collaboration, *The Belle detector*, *Nucl. Instrum. Meth. A* **479** (2002) 117 [INSPIRE].

[13] Belle-II collaboration, *Belle II technical design report*, arXiv:1011.0352 [INSPIRE].

[14] Belle collaboration, *Physics achievements from the Belle experiment*, *PTEP* **2012** (2012) 04D001 [arXiv:1212.5342] [INSPIRE].

[15] S. Kurokawa and E. Kikutani, *Overview of the KEKB accelerators*, *Nucl. Instrum. Meth. A* **499** (2003) 1 [INSPIRE].

[16] T. Abe et al., *Achievements of KEKB*, *PTEP* **2013** (2013) 03A001 [INSPIRE].

JHEP09(2023)146

[17] SuperKEKB collaboration, *SuperKEKB collider*, *Nucl. Instrum. Meth. A* **907** (2018) 188 [arXiv:1809.01958] [INSPIRE].

[18] D.J. Lange, *The EvtGen particle decay simulation package*, *Nucl. Instrum. Meth. A* **462** (2001) 152 [INSPIRE].

[19] T. Sjöstrand, S. Mrenna and P.Z. Skands, *A brief introduction to PYTHIA* 8.1, *Comput. Phys. Commun.* **178** (2008) 852 [arXiv:0710.3820] [INSPIRE].

[20] S. Jadach, B.F.L. Ward and Z. Was, *The precision Monte Carlo event generator KK for two fermion final states in e^+e^- collisions*, *Comput. Phys. Commun.* **130** (2000) 260 [hep-ph/9912214] [INSPIRE].

[21] E. Barberio and Z. Was, *PHOTOS: a universal Monte Carlo for QED radiative corrections. Version* 2.0, *Comput. Phys. Commun.* **79** (1994) 291 [INSPIRE].

[22] R. Brun et al., *GEANT*3, CERN Program Library Long Writeup W5013, CERN-DD-EE-84-1, unpublished (1987) [INSPIRE].

[23] GEANT4 collaboration, *GEANT*4 — *a simulation toolkit*, *Nucl. Instrum. Meth. A* **506** (2003) 250 [INSPIRE].

[24] C. Bernardini et al., *Lifetime and beam size in a storage ring*, *Phys. Rev. Lett.* **10** (1963) 407 [INSPIRE].

[25] P.M. Lewis et al., *First measurements of beam backgrounds at SuperKEKB*, *Nucl. Instrum. Meth. A* **914** (2019) 69 [arXiv:1802.01366] [INSPIRE].

[26] A. Natochii et al., *Measured and projected beam backgrounds in the Belle II experiment at the SuperKEKB collider*, *Nucl. Instrum. Meth. A* **1055** (2023) 168550 [arXiv:2302.01566] [INSPIRE].

[27] M. Gelb et al., *B2BII: data conversion from Belle to Belle II*, *Comput. Softw. Big Sci.* **2** (2018) 9 [arXiv:1810.00019] [INSPIRE].

[28] Belle-II Framework Software Group collaboration, *The Belle II core software*, *Comput. Softw. Big Sci.* **3** (2019) 1 [arXiv:1809.04299] [INSPIRE].

[29] The Belle II collaboration, *Belle II analysis software framework (basf*2*)*, Zenodo (2022) [DOI:10.5281/ZENODO.5574115].

[30] Belle collaboration, *Measurement of time-dependent CP asymmetries in $B^0 \to K^0_S\eta\gamma$ decays*, *Phys. Rev. D* **97** (2018) 092003 [arXiv:1803.07774] [INSPIRE].

[31] T. Keck, *FastBDT: a speed-optimized multivariate classification algorithm for the Belle II experiment*, *Comput. Softw. Big Sci.* **1** (2017) 2 [INSPIRE].

[32] G.C. Fox and S. Wolfram, *Observables for the analysis of event shapes in e^+e^- annihilation and other processes*, *Phys. Rev. Lett.* **41** (1978) 1581 [INSPIRE].

[33] Belle collaboration, *Evidence for $B^0 \to \pi^0\pi^0$*, *Phys. Rev. Lett.* **91** (2003) 261801 [hep-ex/0308040] [INSPIRE].

[34] E. Farhi, *A QCD test for jets*, *Phys. Rev. Lett.* **39** (1977) 1587 [INSPIRE].

[35] Belle collaboration, *Neutral B flavor tagging for the measurement of mixing induced CP violation at Belle*, *Nucl. Instrum. Meth. A* **533** (2004) 516 [hep-ex/0403022] [INSPIRE].

[36] Belle-II collaboration, *B-flavor tagging at Belle II*, *Eur. Phys. J. C* **82** (2022) 283 [arXiv:2110.00790] [INSPIRE].

JHEP09(2023)146